Environmental Fate Modeling of Nanoplastics in a Salinity Gradient Using a Lab-on-a-Chip: Where Does the Nanoscale Fraction of Plastic Debris Accumulate?

Zélie Venel, Hervé Tabuteau, Alice Pradel, Pierre-Yves Pascal, Bruno Grassl, Hind El Hadri, Magalie Baudrimont, Julien Gigault

Environmental fate modelling of nanoplastics in a salinity gradient using lab-on-a-chip: where does the nanoscale fraction of plastic debris accumulate?

Zélie Venel[1,3], Hervé Tabuteau[2]*, Alice Pradel[1], Pierre-Yves Pascal[6], Bruno Grassl[4], Hind El Hadri[4], Magalie Baudrimont[3], Julien Gigault[1,5]*

1 Géosciences Rennes, UMR6118, CNRS/Université de Rennes 1, Rennes, France

2 IPR, UMR6251, CNRS/Université de Rennes 1, Rennes, France

3 EPOC, UMR5805, CNRS/Université de Bordeaux, Bordeaux, France

4 IPREM, UMR5254, CNRS/Université de Pau et des Pays de l'Adour, Pau, France

5 TAKUVIK, UMI3376, CNRS/Université Laval, Québec, Canada

6 UMR 7138 Evolution Paris-Seine, Equipe Biologie de la Mangrove, Laboratoire de Biologie Marine, Université des Antilles, France

*Corresponding author:
julien.gigault@takuvik.ulaval.ca , (ORCID ID: 0000-0002-2988-8942)
herve.tabuteau@univ-rennes1.fr , (ORCID ID: 0000-0001-9885-8192)

Abstract:

The aim of this study is to demonstrate how the flow and diffusion of nanoplastics through a salinity gradient, as observed in mangrove swamps, influence their aggregation pathways. These two parameters have never yet been used to evaluate the fate and behavior of colloids in the environment, since they cannot be incorporated into classical experimental setups. Land-sea continuums, such as estuaries and mangrove swamp systems, are known to be environmentally reactive interfaces that influence the colloidal distribution of pollutants. Using a microfluidic approach to reproduce the salinity gradient, and its dynamics, the results show that nanoplastics arriving in a mangrove swamp are fractionated. First, a substantial fraction rapidly aggregates to reach the micro-scale, principally governed by an orthokinetic aggregation process and diffusiophoresis drift. These large nanoplastic aggregates eventually float near the water's surface or settle into the sediment at the bottom of the mangrove swamp, depending on their density. The second, smaller fraction remains stable and is transported towards the saline environment. This distribution results from the combined action of the spatial salt concentration gradient and orthokinetic aggregation, which is largely underestimated in the literature. Due to nanoplastics' reactive behavior, the present work demonstrates that mangrove and estuarine systems need to be better examined regarding plastic pollution.

Keywords: Nanoplastics; aggregation; salinity; microfluidics; environmental

Introduction

Global hydrodynamic models estimate that hundreds of thousands of tonnes of microplastics, i.e., with sizes ranging from 0.025 mm to a few mm, are likely floating in the oceans, mainly in subtropical gyres where they continuously accumulate, due to sea currents[1–4]. It was recently demonstrated that microplastics can be also generated in terrestrial ecosystems before leaving land and reaching a gigantic gyre through rivers and other hydraulic systems[5]. Despite this better understanding of the source of plastic in the oceans, we still only know where approximately 1% of the mass of plastics deposited on land has ended up.[6]. Clearly, microplastics (<5 mm) are lost somehow during their transportation from lands to the oceans. It was recently demonstrated that during their transportation, plastic debris and microplastics are continuously weathered until they are tiny nanoscale pieces, i.e., nanoplastics[7,8]. There is recent proof of nanoplastics appearing in consumer products and in environmental systems, such as oceans and soils[9–11]. However, due to the lack of appropriate analytical methods to identify and characterize trace concentations of nanoplastics in environmental systems, generally rich in natural and colloidal organic matter, there is very little data on the relative distribution of nanoplastics in the global environment. As with microplastics and other colloids, it is likely that nanoplastics are transported through river and estuarine systems as well[12,13].

The main parameters that influence nanoplastic behavior in saline environments are ionic strength, organic matter, and pH[14–17]. In typical experiments, a given quantity of salt, such as NaCl or $CaCl_2$, is added to a dilute dispersion of nanoplastics, and their aggregation is monitored as soon as the salt concentration becomes homogeneous[18,19]. Using these experimental approaches, the aggregation mechanisms of nanoplastics and the stability of their ionic strength can be characterized, principally through the critical coagulation concentration (CCC). However, these results can not be extrapolated to environmental systems that are experience continuous spatial and temporal variations of natural features (such as the ionic strength), so they cannot be considered at equilibrium[20,21]. In particular, most land-sea continuum systems that nanoplastics are supposed to pass through are characterized by large salinity gradients and high flow rates. These two parameters are never investigated together to evaluate the fate of nanoplastics in the estuarine systems, since they cannot be jointly incorporated and controlled in classical experimental setups. Therefore, the major limitation of

the present experimental approach used to determine the stability/aggregation of nanoplastics is the lack of environmental representativeness.

The present work is focused on the fate of model nanoplastics under flow conditions and with the presence of a salinity gradient (SG). These two conditions are generally encountered in mangrove swamps, which are some of the most fragile and essential ecosystems on Earth. Mangroves are characterized by a strong relationship with the ocean and land with both direct and indirect high anthropogenic pressures[22,23]. These zones remain poorly investigated in terms of their aquatic physical and chemical properties. Based on physical and chemical parameter measurements in a mangrove swamp, the objective of this experiment is to study the nanoplastics aggregation dynamics under some of the specific initial conditions encountered in mangrove swamps when they pass through the salinity gradient. To do so, microfluidic experiments were designed to determine the behavior of nanoplastics under flow in the presence of a salinity gradient. These experiments allow us to (i) control the flow conditions of both the freshwater and the seawater, (ii) establish a spatial salt gradient in the channel, and monitor the diffusiophoretic drift of the nanoplastics due to this SG, and (iii) determine some of the features of the particle aggregation due to the shear flow, i.e., the orthokinetic aggregation. Indeed, it is demonstrated that the nanoplastics aggregation process results from their collision, and not from classical diffusion mechanisms. The new experimental results presented can be extrapolated to a mangrove swamp and open the door to new questions concerning these estuarine and coastal systems regarding the environmental behavior and impact of nanoplastics.

Materials and Methods

Chemical and sample preparation

Polystyrene nanoplastics (PS-nanoplastics) were synthesized to be representative (size and shape) of environmental nanoplastics as previously described[24]. PS-nanoplastics were formed using polystyrene pellets that are crushed by a ball-milling process. Such hydrophobic materials generally form carbon-based nanoplastics with a low surface charge. The *z*-average hydrodynamic diameter (d_{zH}) of the PS-nanoplastics is centered at 380-400 nm, and they are highly polydispersed. Moreover, despite having a zeta potential of –32 mV in an aqueous system at pH 7 and low ionic strength, a relatively low -COOH functional concentration (0.5 mmol g^{-1}) was measured[24]. No surfactants or other additives were present in the dispersing media.

Mangrove observation and analysis

Based on a previous study, nanoplastics were identified on Guadeloupe (a French Caribbean island) on beaches exposed to the North Atlantic gyre[25]. It has been identified that some of the

debris comes directly from the garbage of the inhabitants of the island, as it comes from the largest open landfill on the island, the Gabarre landfill. This landfill is located between the city of Pointe-à-Pitres in the south and a large surrounding mangrove area, as illustrated on Fig. 1.

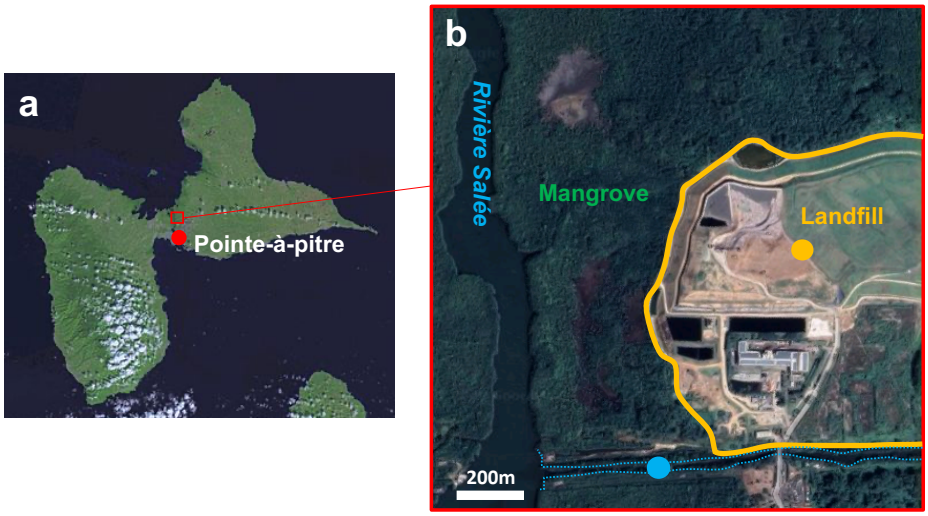

Figure 1: (a) Location of the sampling zone on the French Caribbean island of Guadeloupe. (b) Detail of the landfill in the mangrove swamp and the sampling location point (GPS coordinates of the blue point: 16°15'20.2"N 61°32'39.6"W)

There is a landfill located near the mangrove swamp's "rivière salée" or saline estuary, which leaches anthropogenic colloids and other landfill leachate into the estuary, which is the main channel of the mangrove swamp. In addition, the mangrove area is the contact area between the leached freshwater and the inundation of seawater. However, there is no precise information about salt distribution in the mangrove swamp (MSP), particularly inside the saline estuary that flows across the mangrove area. The salinity was measured (in October 30th 2019) using an in situ conductimeter near one arm of the river that is close to the landfill (Fig. 2.b, blue point). The salinity and temperature profile of the mangrove area water column were measured using in situ conductimeters (Ijinus, Quimperlé, France). Briefly, eight conductimeter sensors were placed along a 1.5 m *z*-axis arm and fixed to a boat. The total depth of the river arm was approximately 2 m. Measurements were performed over half of a tidal cycle, starting at the end of the afternoon and ending early the following morning. The mangrove swamp current was analyzed using a current meter (homemade setup). Due to their high affinity with colloids, the colloidal Cu(II) concentration was measured as a proxy of colloid presence in estuarine systems such as the mangrove swamp [26,27]. It was demonstrated that the size distribution of Cu(II) with colloids varied between marine systems and fresh water[28]. A change in the relative size fraction

of Cu(II) is therefore a releavant proxy of nanoplastics, especially since they are expected to be disseminated/mixed through the movement of natural and other anthropogenic colloids. Water samples were collected at different depths and Cu(II) was analyzed after preliminary sequential ultrafiltration using Amicon cell (Millipore, France) and a polyethersulfonated membrane (NADIR, Alting, France) with a molecular weight cut-off of 10kDa. Cu was analyzed by Inductively Coupled-Plasma Mass Spectrometry (7700x, Agilent Technologies, France).

Size and charge characterization

Hydrodynamic diameters (d_H) were determined by in situ dynamic light scattering (DLS) using a Vasco-Flex model particle size analyzer (Cordouan Technologies). Each DLS measurement corresponded to an average of six measurements of 60 seconds each. Each sample was assigned a Z-average hydrodynamic diameter (d_{zH}) using a cumulant algorithm. Additionally, the sparse Bayesian learning (SBL) algorithm was used to obtain the size distribution. All results presented have less than a 1% difference between all the points of the raw and fitted autocorrelation function. The size of large aggregates deposited on top of the microfluidic device (MD) was also evaluated using optical microscopy (Leica, France). The aggregate sizes were measured using ImageJ software.

Transport in the microfluidic devices

In the present work, to simulate the fate of nanoplastics that were initially transported by the fresh water that enters the mangrove swamp from inland, an experimental approach was based on a microfluidic set up. As previously described, a microfluidic device was developed to mimic a salinity gradient[29]. The working principle is summarized in Figure 2. Two inlet and outlet arms of 5 mm long and 200 µm wide were connected to a 1.7 cm long, 800 µm wide channel. The height of the arms and channels was 75 µm. Aqueous dispersions of nanoplastics and NaCl solution were injected together in the two different inlets of the microfluidic device using syringe pumps (KDS 200 scientific) at the same flow rate Q (from 0.5 to 10 mL h^{-1}). This range of average fluid velocity in the microfluidic device corresponds to the average fluid velocity within the water column that was measured at our sampling site and in the greater mangrove area[30]. Concerning the inlets, PS-nanoplastics dispersion (in deionized water) are injected into Inlet A, named A_{in}, while the NaCl solution is injected through Inlet B, named B_{in}. The outlets are named A_{out} and B_{out}. A_{out} and A_{in} are arranged on the same side of the device, where PS-nanoplastics are principally eluted, and the same is true of B_{out} and B_{in} for the NaCl

solution. According to the MD dimensions and the flow rates investigated, all experiments were performed at a low Reynold number ($0.02<Re<0.4$) and with a Péclet number higher than 10^4, meaning that the nanoplastics did not diffuse around the fluid streamlines more than a few micrometers transverse to the flow direction over the whole length of the device. The liquids flowed through 20 cm tubing with an inner diameter of 360 µm before being collected in two vials connected to each outlet for one hour. Then, the flow was stopped, and the evolution of the d_{zH} for the nanoplastics was monitored over 100 min using the in situ DLS probe. The device was first saturated with pure water and then filled with a 500 mM NaCl concentration from one inlet and PS-nanoplastics dispersion from the other. The final conductivity and NaCl concentration were measured at both outlets, A_{out} and B_{out}, for the different flow rates. The NaCl concentration ranged from 30 to 108 mM in A_{out} for decreasing Q (mL min^{-1}), while it ranged from 390 to 470 mM in B_{out} for increasing Q (see SI, Fig. S3c). The evolution of the salt concentration in the vials indicates that salt diffusion occurred in the A_{out}.

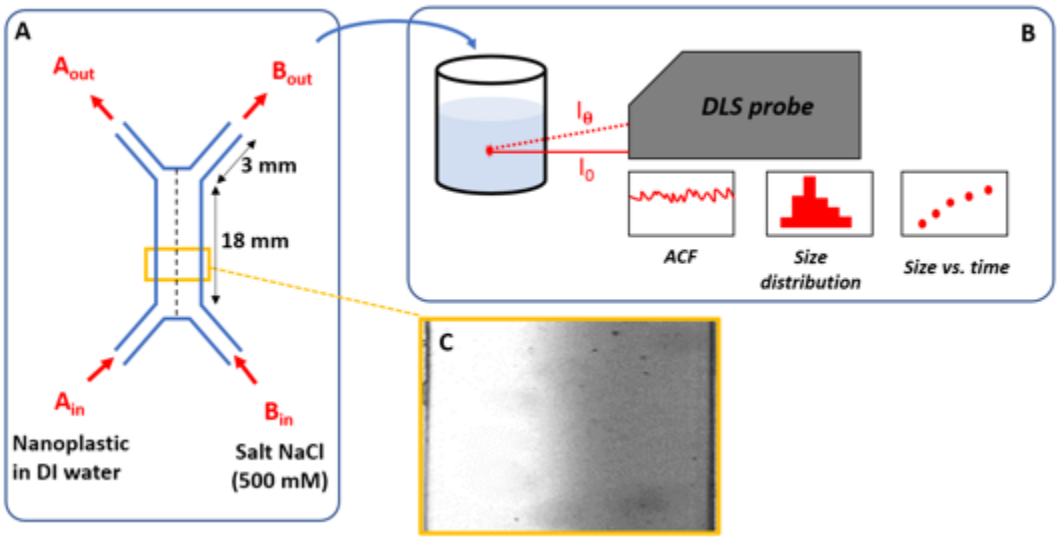

Figure 2: (a) Sketch of the experimental conditions in the microfluidic device (MD). After the nanoplastics flow through the MD, they flow through the tubing and are eventually collected in vials. (b) DLS allowed us to determine the evolution of the aggregate size over time. (c) View of the interface between the nanoplastic suspension (left) and a patent blue V dye suspension with the same diffusion coefficient as that of the saline suspension. The variation in the gray level across the channel allowed us to determine the salt concentration profile averaged over the height of the MD after a calibration experiment. This profile image is from an experiment with Q=2 ml h^{-1} and was taken in the middle of the straight part of the MD.

Aggregation kinetics: theory and batch experiments

Nanoplastic aggregation kinetics were determined using the classical approach developed by Smoluchowski (Smoluchowski 1917). According to this theory, this is a two-step process: collision and attachment, which are determined by the collision rate constants and the

attachment efficiency α, respectively. The evolution of the PS-nanoplastics concentration over time can be expressed as:

$$\frac{dN_k}{dt} = \frac{\alpha}{2}\sum_{i+j\to k}\beta_{ij}N_iN_k - \alpha N_k\sum_i \beta_{ik}N_i \qquad \text{(Eq. 1)}$$

where k is the mass of aggregate and N is the number of particles in the aggregate. β_{ij} is the collision frequency between two nanoplastics of different sizes with masses of i and j. For the colloidal population, β_{ij} is directly controlled by Brownian diffusion. In the case of homoaggregation, the equation is:

$$\frac{dN_k}{dt} = -\alpha\beta_{kk}\left(\frac{N_k}{2}\right)^2 \qquad \text{(Eq. 2)}$$

The aggregation rate is determined by the slope in the linear part of the aggregation curve $d_{zH}=f(t)$. The attachment efficiency α can be obtained by calculating the aggregation rate at different electrolyte concentrations. The ratio between the aggregation rate in favorable conditions (k_{fast}, generally at high ionic strength, > critical coagulation concentration) and unfavorable conditions (k_{slow}), normalized by the initial particulate concentration N_0, allows the determination of α[31] and is expressed as:

$$\alpha = \frac{k_{slow}}{k_{fast}} = \frac{\frac{1}{N_0}\left(\frac{dr_p}{dt}\right)_{t\to 0}}{\frac{1}{N_{0,fast}}\left(\frac{dr_p}{dt}\right)_{t\to 0,fast}} \qquad \text{(Eq. 3)}$$

In the case of total aggregation, the attachment coefficient (α = 1) and the aggregation rate are solely dependent on the efficiency of transport. In batch mode experiments, NaCl is periodically injected into a closed and finite volume containing the nanoplastics. By measuring the z-average hydrodynamic diameter (d_{zH}) over time, it is therefore possible to determine the aggregation kinetics. As illustrated elsewhere[32,33], steric and physical rearrangements lead to the formation of compact aggregates even for the diffusion-limited aggregation (DLA) mode.

Results & Discussion

Persistence of the salinity gradient in the mangrove swamp

Figure 3 shows the temporal variation in the salinity and the temperature profile along the depth of the column. As expected, those variations are not the same in a rising tide and in a falling tide. For the rising tide, two depth zones were distinguished that had distinct salt concentrations

(Fig. 3, Zone 2). In the first zone, in the first 0.5-0.75 m below the surface there is a salinity gradient, while deeper in the second zone, over 1 m, the salt concentration is rather homogeneous. These changes in salt concentration are directly linked to the incoming flows in this arm of the "rivière salée" (saline estuary) during the rising tide. While there is a continuous flux of fresh water from the east to the west, the seawater flows in the opposite direction. It invades the river arm below the surface at a depth of approximately 0.5-0.75 m below the surface, the depth at which the salt concentration is hence the highest. Further into the river, and farther from its connection to the saline estuary the slope of the SG decreases (Fig. S1). During the inundation process, the salt contained in this finger of seawater diffuses into the two zones: from surface to –50cm depth and from –50cm to –150cm. Since the flow rate of freshwater in the first zone is faster than that in the second zone, the diffusion of salt is less important in this zone and leads to the formation of the salinity gradient that spreads throughout the first zone. In the second zone, salt diffusion occurs more quickly, the flow rate is slower, and a more or less homogeneous salt concentration develops rapidly.

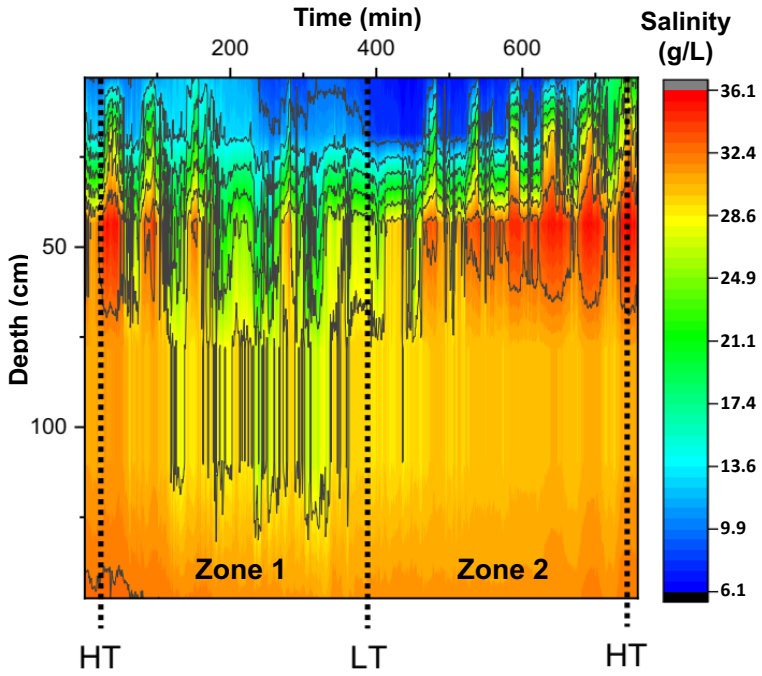

Figure 3: Temporal evolution of the salinity gradient along 1.5 m of water from the surface of the water. HT and LT correspond to high and low tide, respectively, while Zones 1 and 2 are the falling and rising phases of the tide.

During the falling tide (Fig. 3, Zone 1), as less seawater gushes in, the amount of salt coming from the seawater decreases rapidly, which leads to a broadening of the salinity gradient to almost 1.5 m. The salinity gradient of the falling tide is smoother than in the rising tide, with a maximum salt concentration of approximately 28 g L^{-1}, instead of 36 g L^{-1}. It is worth noting that in both tide phases, the salt profile oscillates periodically, approximately every 40 min,

which changes the position of the maximum salt concentration. As a result, the SG is alternately stretched and compressed, a phenomenon for which no physical explanation has been reported in the literature yet. From all these results, in the river arm, there is always a salinity gradient above the first 0.5-1 m in depth, and thus, there is no global mixing phenomenon that would lead to a homogeneous salt concentration.

This is the first time that such a salinity profile for a mangrove swamp has been obtained, opening new ways of thinking about the fate of colloidal suspensions that are present in the study area. In particular, it is interesting to study what will happen when nanoplastics produced in the landfill are transported through the soil[34] and reach the mangrove swamp. The colloidal Cu(II) concentrations were measured at 3.2 ng g^{-1}, 7.7 ng g^{-1} and 2.7 ng g^{-1} Cu at depths of 0 cm, 50 cm and 100 cm, respectively (see SI, Fig. S1). Clearly, a relative increase of the colloid concentration in the salinity gradient zone (30-50 cm) was observed, raising key questions about the fate and transport of nanoplastics from the land to the sea and through the mangrove area in between them.

Prior to microfluidic experiments, aggregation kinetics experiments were performed in batch-mode conditions for the PS-nanoplastics, as detailed in the supplemental information (Fig. S2). All these dispersion conditions and physical-chemical properties can explain the low critical coagulation concentration (CCC) value, which was around 30 mM. In the experiments, a salt concentration higher than the CCC was always used and only the concentration of the nanoplastics was varied. As expected, the mean aggregate size increased with the particle concentration (Fig. S2). The aggregate size varied linearly over time for particle concentrations from 1 to 11 mg L^{-1}. The dependence of the aggregation rate on the particle concentration is coherent with Equation (2) and is explained by the probability of collision between nanoplastics and aggregates. Under these experimental conditions, the aggregation is driven by particle diffusion, i.e., the DLA mode for which the attachment coefficient α is strongly dependent on the collision frequency β_{kk}. At lower concentrations, the aggregation is rather limited, and the largest aggregates are doublets or triplets, while most of the nanoplastics remain isolated. Under these conditions, as expected, the aggregate size varied linearly over time.

Based on these batch experiments, different investigations have been tried using microfluidic devices, with the same nanoplastics concentration variation as summarized in Figure 4. During all the MD experiments, nanoplastics deposition was observed near the middle of the main channel along the flow direction (Fig. 4a), and the deposited nanoplastics included relatively large micrometric aggregates (Fig. 4.b). This deposition occurred inside a band whose width corresponded to the extension of the salinity gradient perpendicular to the flow direction. The

position of this gradient depended on the flow rate and the Brownian diffusion of salt across the flow stream lines. The relevant length scale for this diffusion process for the salt was the saturation mixing length, $l_s = w^2 . U/D_s$, with w is the width and h is the height of the MD, U as the average velocity of the flow and D_s as the diffusion coefficient of the salt (D_S= 1.52 10^{-9} m^2 s^{-1}). Here, the channel is much wider than it is tall, $w>>h$, so the salt diffuses first across the height of the channel as it enters the main channel and flows over the first micrometers. Thereafter, it diffused across the width of the channel, perpendicular to the flow direction, until the salt water had reached the entire channel width. During this diffusion process, the salt moved by advection in the flow direction over a distance equal to l_s from the entrance. Beyond this distance, the profile of the salt concentration in the MD cross-section did not continue to change further downstream. In our experimental conditions, the smallest value of l_s was equal to 0.78 m, which is much greater than the length of the main channel of the MD for all the flow rates. Therefore, the salt had not moved across the whole width of the MD as it came out of the main channel. As a result, there was a constant broadening of the deposition band further downstream up to the exit zone of the main channel (Fig. 4). Inside this deposition band, the salt concentration was higher than the CCC of the nanoplastics, which thus enhanced their aggregation and successive deposition (Fig. 4a).

Nanoplastics deposition also occurred in both outlet arms. This process is more important in the outlet arms than in the main channel, since the salt concentration is consistently higher than the CCC and the particle concentration is higher. Since the Péclet number, Pe, with this Q range was always higher than 10^4, nanoplastics scarcely diffused as they flowed through the MD. Hence, particle aggregation in the whole MD was not due to particle diffusion, but rather to particle collisions that are transported to adjacent fluid streamlines with different velocities. If the collisions are caused by hydrodynamic motions (e.g convection or sedimentation) this is then referred to as orthokinetic aggregation. This process, called orthokinetic aggregation, is enhanced since the nanoplastics have no electrostatic barrier due to the high salt concentration.

However, the internal diameter of this tubing is equal to 360 µm, and the associated Pe number is comparable to that of the MD; therefore, there was also particle aggregation due to collisions and subsequent deposition in the tubing. The length of the tubing is approximately 20 cm, 10 times longer than the length of the main channel and the outlet arm of the MD; thus, most of the nanoplastics that exit the MD float, and are deposited at the top of the tubing. From the ratio between the length of the MD and that of the tubing, it was found that 90% of the particle aggregation takes place in the tubing. It is worth noting that nanoplastics deposition in the

outlet, where only the saline solution is supposed to flow, is the result of the coupling of the salt migration and the diffusiophoretic drift of the nanoplastics[35]. The diffusiophoresis is defined as the spontaneous motion of colloidal particles or molecules in a fluid induced by a concentration gradient of a different substance, as previously explained in controlled microfluidic experiments but not yet observed and characterized in the environment[36]. This result suggests that there will be significant aggregation of nanoplastics in such places if the salt concentration is locally high enough to completely or partially screen the surface charge of the PS-nanoplastics.

Indeed, nanoplastics tended to accumulate near the region where the salt concentration is the highest. Due to the salt diffusion in the part of the channel where the nanoplastics flowed, the maximum salt concentration (MSC) was not located at the middle of the channel in the flow direction but inside the saline part of the channel (Fig. 4a). Therefore, the accumulated nanoplastics near the MSC will eventually come out of the MD through outlet B_{out} and not by A_{out}. Since the salt diffusion across the channel is higher at lower flow rates (Fig. S3), the location of the MSC is further inside the saline part of the channel, and thus, even more nanoplastics flow through the outlet B_{out}.

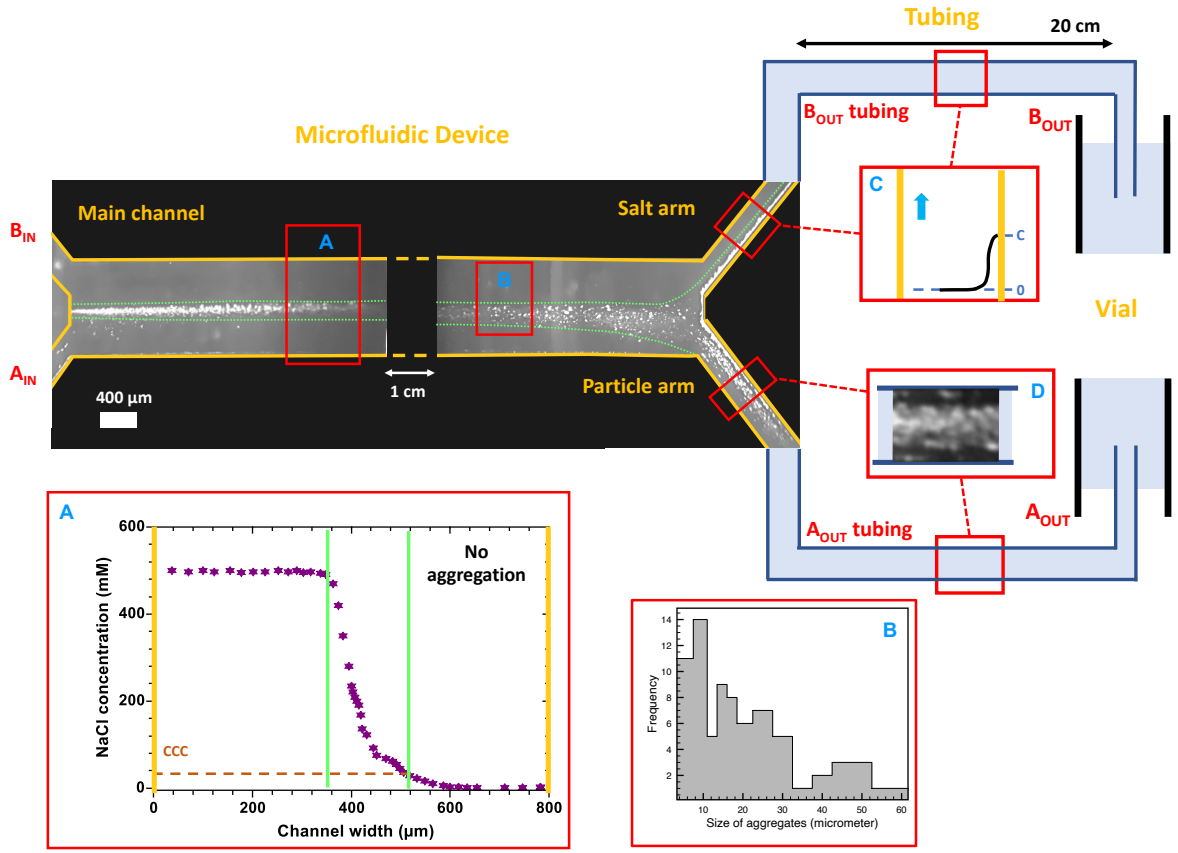

Figure 4: Microfluidic device (MD) experiment. (Top left) Image of the main straight part of the MD and the two outlet arms. Tubing connects the outlet to the vial. (A) Salt concentration profile along the width of the MD. The two yellow and green lines (color online) correspond to the lateral walls of the MD and to the salinity gradient in which the salt concentration is higher than the CCC, respectively. (B) Size distribution of the aggregates deposited on the top wall of the MD. (C) Concentration profile of the nanoplastics in the B_{out} arm and tubing. (D) Image of the colloidal deposit in the A_{out} arm and tubing. The blue arrows in 1 and 3 indicate the flow direction.

The impact of the particle aggregation and deposition in the MD and in the tubing was measured in the vials through DLS measurements (Fig. 5). It is worth noting that there was no fluid agitation in the vial. Therefore, if particle aggregation takes place in the vials, it is only due to Brownian diffusion. In the A_{out} vial, since the ionic strength was always higher than the CCC, regardless of the flow rate, the particle concentration is assumed to be high enough to observe particle aggregation, as in the batch experiments. However, the aggregation process in the vial was much more limited than that in the batch experiments (Fig. S2b). There was almost no aggregation for $2< Q <10$ mL/h and a slight increase in the aggregate size, up to $1.3D_i$, for the two lowest Q values (0.5 and 1 mL/h), with D_i being the initial particle size (i.e. before injection to the microfluidic device), while in the batch experiments, the mean aggregate size was approximately $3D_i$ at a similar concentration and constantly increased.

The results for vial B_{out} are even more surprising, since aggregation occurred irrespective of the flow rate (Fig. 5), even if nanoplastics were not supposed to be present in this vial. Again, with a salt concentration well above the CCC ($I > 470$ mmol L^{-1}) for all Q values, the mean aggregate size was smaller than in the batch experiments, except at the lowest flow rate. In this last case, the aggregate size ranged from 1.5 to $3D_i$ after 120 min. Together, these measurements of the aggregate size in the vials suggest that the amount of nanoplastics that are lost in the MD and in the tubing is determined by a two-step process. First, there is a massive aggregation process that takes place in the bulk of the fluid, due to the collisions either between individual nanoplastics or between nanoplastics and aggregates, since the *Pe* number is high enough to consider that the aggregation is mostly orthokinetic, and the particle diffusion is negligible. In the second step, the aggregates that are close to the surface either migrate towards the wall due to the higher salt concentration near the surface[37], or are captured by physical interception by other immobile aggregates that lie on the surface. Based on a previous study on PS-nanoplastics[24], large micrometric aggregates of PS-nanoplastics mainly float and therefore are located near the top walls. Nanoplastics may also sink into the sediment at the bottom, since a substantial fraction of plastics are heavier than the seawater, as demonstrated in a previous study with fullerenes[29]. Since the mean size of the deposited aggregates was quite large, this result may suppose that the flow does not fragment many of the aggregates, meaning that they have both great internal cohesion and strong adhesion on the surface of the PDMS, which the MD is made of [38], preventing them from being broken by shear forces.

This deposition process mainly occurred inside the tubing, and it is so important that there were not enough nanoplastics in the vials to observe significant aggregation by diffusion. Even though aggregation can occur, the nanoplastics can form only very small aggregates (doublets,

triplets) that are far from each other, and the DLS signal is still dominated by the individual nanoplastics. By comparison with the aggregate size evolution in the batch with a low particle concentration, it was estimated that the maximum amount of nanoplastics obtained at the lowest flow rate was approximately 1-2 and 10% in A_{out} and B_{out}, respectively, of the number of nanoplastics that were initially injected into the MD (Fig. S3).

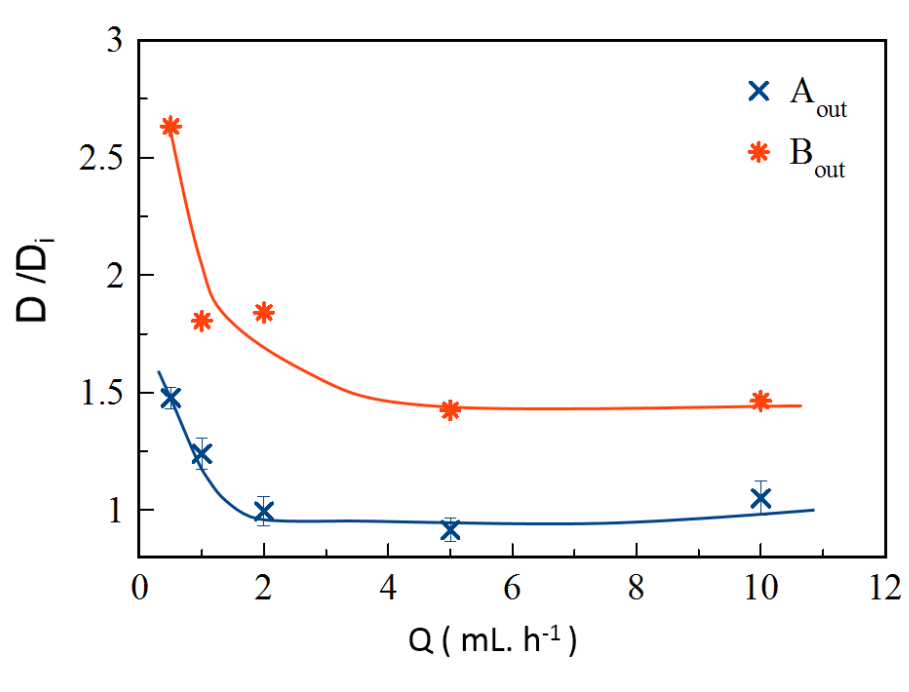

Figure 5: Variation in the mean aggregate size, scaled by the initial size of the nanoplastics, with the flow rate for the two outlets.

In order to extrapolate these results to mangrove swamps, two relevant time and length scales of particle transport in the microfluidic device were considered. First, the residence time inside the MD, and thereafter in the tubing, for the PS-nanoplastics that eventually reached the vials was between 4 and 80 seconds, depending on the flow rate. Everything happens on this short time scale where the aggregation induced by the SG is much faster than in the batch. Over longer times, this phenomenon will integrate all these aggregations throughout a mangrove swamp. As a result, only a small fraction of PS-nanoplastics, those which have not aggregated or slightly aggregated, will be released into the ocean, and the majority will remain flocculated (either floating or sunk to the sediment in various forms) in the mangroves (associated with natural colloids, sediment etc). Indeed, the results suggest that PS-nanoplastics will remain in the mangrove area for a much longer time, even though the average flow rate may be faster than that in the MD, since the mangrove swamp is much larger than the MD. This longer residence time will greatly increase the probability of the PS-nanoplastics to become involved in aggregation processes with either other PS-nanoplastics of the same type or, more likely,

with the rest of the colloidal matter in suspension, in particular with organic matter. This longer residence time will also favor NP aggregation, since it will increase the diffusiophoretic drift of the PS-nanoplastics towards the high salt concentration zone in the water column, which will lead to a decrease in the surface charge of the nanoplastics.

Second, the growing aggregates cannot move more than 35-180 μm before becoming attached to the microfluidic device or the tubing walls. Therefore, aggregates cannot substantially grow in size before becoming immobile on a wall, i.e., they do not encounter more than one or two other nanoplastics/aggregates during their floating/sedimentation. In the mangrove area, the salt concentration is high at depths from tens of centimeters up to a few meters, which is at least three orders of magnitude deeper than the depth of the microfluidic experiment. Therefore, it is expected that in a mangrove swamp, the average mean size of the aggregate can become much greater than in the MD, since the aggregate can encounter many other aggregates as they either sediment or float. In addition, the collision rate increases as the mean aggregate size increases, since larger aggregates have a greater surface area and thus a higher chance of colliding with another aggregate.

The results obtained demonstrate that the salinity gradient, and therefore mangrove swamps, act as a separator for nanoplastics according to their aggregation pathways. However, contrary to classical approaches, it was demonstrated that nanoplastic aggregation is driven by an orthokinetic process induced by the flow and the SG together. Indeed, all the aggregates formed in the SG will eventually either float to the surface, or settle down to the sediment in the MD or in the tubing, and only single nanoplastics and small aggregates are able to reach the vials. This rough analysis seems to suggest that PS-nanoplastics and especially nanoplastics that enter the mangrove swamp from land-based sources would be filtered, and that only a small fraction would reach the oceanic system as either nanoscale or microscale floating aggregates of nanoplastics. However, ongoing studies on the aggregation mechanisms of PS-nanoplastics in the mangrove swamp are performed considering the implication of turbulence and the natural organic matter in the MD. Indeed, such parameters could definitely play a role in the ortho-kinetic aggregation process along their transportation in the salinity gradient of the mangrove swamp. New sampling strategies need to be developed to detect (hetero-) aggregates of PS-nanoplastics, taking into account the specific characteristics of these substances that lead to their different reactivities with contaminants and the other natural components. Finally, the results show the importance of protecting coastal mangrove ecosystems, since, apart from protecting the coast from possible storms and acting as habitat for terrestrial and aquatic species, they also act as natural filters and concentrator sinks for nanoplastics.

Supporting Information. Description of the sampling points in the Mangrove (Figure S1); Size and stability evaluation of the nanoplastics model (Figure S2); Size evolution of nanoplastics model in the microfluidic device (Figure S3); NaCl distribution in the microfluidic

device (Figure S4); Size evolution of spherical polystyrene nanoparticles in batch and microfluidic experiments (Figure S5).

Acknowledgments

We acknowledge funding and support from the French Agency for Research - ANR (ANR-17-CE34-0008). We acknowledge Sebastien Cordonnier for technical support in the Mangrove swamp.

References

(1) Eriksen, M.; Lebreton, L. C. M.; Carson, H. S.; Thiel, M.; Moore, C. J.; Borerro, J. C.; Galgani, F.; Ryan, P. G.; Reisser, J. Plastic Pollution in the World's Oceans: More than 5 Trillion Plastic Pieces Weighing over 250,000 Tons Afloat at Sea. *PLOS ONE* **2014**, *9* (12), e111913. https://doi.org/10.1371/journal.pone.0111913.
(2) Andrady, A. L. Microplastics in the Marine Environment. *Mar. Pollut. Bull.* **2011**, *62* (8), 1596–1605. https://doi.org/10.1016/j.marpolbul.2011.05.030.
(3) Cózar, A.; Echevarría, F.; González-Gordillo, J. I.; Irigoien, X.; Úbeda, B.; Hernández-León, S.; Palma, Á. T.; Navarro, S.; García-de-Lomas, J.; Ruiz, A.; Fernández-de-Puelles, M. L.; Duarte, C. M. Plastic Debris in the Open Ocean. *Proc. Natl. Acad. Sci.* **2014**, *111* (28), 10239–10244. https://doi.org/10.1073/pnas.1314705111.
(4) Jambeck, J. R.; Geyer, R.; Wilcox, C.; Siegler, T. R.; Perryman, M.; Andrady, A.; Narayan, R.; Law, K. L. Plastic Waste Inputs from Land into the Ocean. *Science* **2015**, *347* (6223), 768–771. https://doi.org/10.1126/science.1260352.
(5) Schmidt, C.; Krauth, T.; Wagner, S. Export of Plastic Debris by Rivers into the Sea. *Environ. Sci. Technol.* **2017**, *51* (21), 12246–12253. https://doi.org/10.1021/acs.est.7b02368.
(6) Sebille, E. van; Wilcox, C.; Lebreton, L.; Maximenko, N.; Hardesty, B. D.; Franeker, J. A. van; Eriksen, M.; Siegel, D.; Galgani, F.; Law, K. L. A Global Inventory of Small Floating Plastic Debris. *Environ. Res. Lett.* **2015**, *10* (12), 124006. https://doi.org/10.1088/1748-9326/10/12/124006.
(7) Lambert, S.; Wagner, M. Characterisation of Nanoplastics during the Degradation of Polystyrene. *Chemosphere* **2016**, *145*, 265–268. https://doi.org/10.1016/j.chemosphere.2015.11.078.
(8) Gigault, J.; Pedrono, B.; Maxit, B.; Halle, A. T. Marine Plastic Litter: The Unanalyzed Nano-Fraction. *Environ. Sci. Nano* **2016**, *3*, 346–350.
(9) Hernandez, L. M.; Xu, E. G.; Larsson, H. C. E.; Tahara, R.; Maisuria, V. B.; Tufenkji, N. Plastic Teabags Release Billions of Microparticles and Nanoparticles into Tea. *Environ. Sci. Technol.* **2019**, *53* (21), 12300–12310. https://doi.org/10.1021/acs.est.9b02540.
(10) Ter Halle, A.; Jeanneau, L.; Martignac, M.; Jardé, E.; Pedrono, B.; Brach, L.; Gigault, J. Nanoplastic in the North Atlantic Subtropical Gyre. *Environ. Sci. Technol.* **2017**, *51* (23), 13689–13697. https://doi.org/10.1021/acs.est.7b03667.
(11) Watteau, F.; Dignac, M.-F.; Bouchard, A.; Revallier, A.; Houot, S. Microplastic Detection in Soil Amended With Municipal Solid Waste Composts as Revealed by Transmission Electronic Microscopy and Pyrolysis/GC/MS. *Front. Sustain. Food Syst.* **2018**, *2*, 81. https://doi.org/10.3389/fsufs.2018.00081.
(12) Dai, M.; Martin, J.-M.; Cauwet, G. The Significant Role of Colloids in the Transport

and Transformation of Organic Carbon and Associated Trace Metals (Cd, Cu and Ni) in the Rhône Delta (France). *Mar. Chem.* **1995**, *51* (2), 159–175. https://doi.org/10.1016/0304-4203(95)00051-R.
(13) Pokrovsky, O. S.; Schott, J. Iron Colloids/Organic Matter Associated Transport of Major and Trace Elements in Small Boreal Rivers and Their Estuaries (NW Russia). *Chem. Geol.* **2002**, *190* (1), 141–179. https://doi.org/10.1016/S0009-2541(02)00115-8.
(14) Hotze, E. M.; Phenrat, T.; Lowry, G. V. Nanoparticle Aggregation: Challenges to Understanding Transport and Reactivity in the Environment. *J. Environ. Qual.* **2010**, *39* (6), 1909–1924.
(15) Lowry, G. V.; Hotze, E. M.; Bernhardt, E. S.; Dionysiou, D. D.; Pedersen, J. A.; Wiesner, M. R.; Xing, B. Environmental Occurrences, Behavior, Fate, and Ecological Effects of Nanomaterials: An Introduction to the Special Series. *J. Environ. Qual.* **2010**, *39* (6), 1867–1874.
(16) Petosa, A. R.; Jaisi, D. P.; Quevedo, I. R.; Elimelech, M.; Tufenkji, N. Aggregation and Deposition of Engineered Nanomaterials in Aquatic Environments: Role of Physicochemical Interactions. *Environ. Sci. Technol.* **2010**, *44* (17), 6532–6549. https://doi.org/10.1021/es100598h.
(17) Alimi, O. S.; Farner Budarz, J.; Hernandez, L. M.; Tufenkji, N. Microplastics and Nanoplastics in Aquatic Environments: Aggregation, Deposition, and Enhanced Contaminant Transport. *Environ. Sci. Technol.* **2018**, *52* (4), 1704–1724. https://doi.org/10.1021/acs.est.7b05559.
(18) Chen, C.-S.; Le, C.; Chiu, M.-H.; Chin, W.-C. The Impact of Nanoplastics on Marine Dissolved Organic Matter Assembly. *Sci. Total Environ.* **2018**, *634*, 316–320. https://doi.org/10.1016/j.scitotenv.2018.03.269.
(19) Oriekhova, O.; Stoll, S. Heteroaggregation of Nanoplastic Particles in the Presence of Inorganic Colloids and Natural Organic Matter. *Environ. Sci. Nano* **2018**, *5* (3), 792–799. https://doi.org/10.1039/c7en01119a.
(20) Saleh, N. B.; Afrooz, A. R. M. N.; Aich, N.; Plazas-Tuttle, J. Aggregation Kinetics and Fractal Dimensions of Nanomaterials in Environmental Systems. In *Engineered Nanoparticles and the Environment: Biophysicochemical Processes and Toxicity*; John Wiley & Sons, Ltd, 2016; pp 139–159. https://doi.org/10.1002/9781119275855.ch8.
(21) Jungblut, S.; Joswig, J.-O.; Eychmüller, A. Diffusion- and Reaction-Limited Cluster Aggregation Revisited †Electronic Supplementary Information (ESI) Available: Demonstrates That the Local Structure of the Aggregates Is Independent of the Volume Fraction of Particles Initially Present in the System. See DOI: 10.1039/C9cp00549h. *Phys. Chem. Chem. Phys.* **2019**, *21* (10), 5723–5729. https://doi.org/10.1039/c9cp00549h.
(22) Giri, C.; Ochieng, E.; Tieszen, L. L.; Zhu, Z.; Singh, A.; Loveland, T.; Masek, J.; Duke, N. Status and Distribution of Mangrove Forests of the World Using Earth Observation Satellite Data. *Glob. Ecol. Biogeogr.* **2011**, *20* (1), 154–159. https://doi.org/10.1111/j.1466-8238.2010.00584.x.
(23) Abuodha, P. A. W.; Kairo, J. G. Human-Induced Stresses on Mangrove Swamps along the Kenyan Coast. *Hydrobiologia* **2001**, *458*, 255–265. https://doi.org/10.1023/A:1013130916811.
(24) El Hadri, H.; Gigault, J.; Maxit, B.; Grassl, B.; Reynaud, S. Nanoplastic from Mechanically Degraded Primary and Secondary Microplastics for Environmental Assessments. *NanoImpact* **2020**, *17*, 100206. https://doi.org/10.1016/j.impact.2019.100206.
(25) Davranche, M.; Lory, C.; Juge, C. L.; Blancho, F.; Dia, A.; Grassl, B.; El Hadri, H.; Pascal, P.-Y.; Gigault, J. Nanoplastics on the Coast Exposed to the North Atlantic Gyre: Evidence and Traceability. *NanoImpact* **2020**, 100262. https://doi.org/10.1016/j.impact.2020.100262.

(26) Shafer, M. M.; Hoffmann, S. R.; Overdier, J. T.; Armstrong, D. E. Physical and Kinetic Speciation of Copper and Zinc in Three Geochemically Contrasting Marine Estuaries. *Environ. Sci. Technol.* **2004**, *38* (14), 3810–3819. https://doi.org/10.1021/es0306765.
(27) Hoffmann, S. R.; Shafer, M. M.; Armstrong, D. E. Strong Colloidal and Dissolved Organic Ligands Binding Copper and Zinc in Rivers. *Environ. Sci. Technol.* **2007**, *41* (20), 6996–7002. https://doi.org/10.1021/es070958v.
(28) Roshan, S.; Wu, J. Dissolved and Colloidal Copper in the Tropical South Pacific. *Geochim. Cosmochim. Acta* **2018**, *233*, 81–94. https://doi.org/10.1016/j.gca.2018.05.008.
(29) Gigault, J.; Balaresque, M.; Tabuteau, H. Estuary-on-a-Chip: Unexpected Results for the Fate and Transport of Nanoparticles. *Environ. Sci. Nano* **2018**, *5* (5), 1231–1236. https://doi.org/10.1039/c8en00184g.
(30) McLachlan, R. L.; Ogston, A. S.; Asp, N. E.; Fricke, A. T.; Nittrouer, C. A.; Gomes, V. J. C. Impacts of Tidal-Channel Connectivity on Transport Asymmetry and Sediment Exchange with Mangrove Forests. *Estuar. Coast. Shelf Sci.* **2020**, *233*, 106524. https://doi.org/10.1016/j.ecss.2019.106524.
(31) Chen, K. L.; Elimelech, M. Influence of Humic Acid on the Aggregation Kinetics of Fullerene (C60) Nanoparticles in Monovalent and Divalent Electrolyte Solutions. *J. Colloid Interface Sci.* **2007**, *309* (1), 126–134. https://doi.org/10.1016/j.jcis.2007.01.074.
(32) Ossadnik, P.; Lam, C.-H.; Sander, L. M. Nonuniversal Diffusion-Limited Aggregation and Exact Fractal Dimensions. *Phys. Rev. E* **1994**, *49* (3), R1788–R1791. https://doi.org/10.1103/PhysRevE.49.R1788.
(33) Meng, Z.; Hashmi, S. M.; Elimelech, M. Aggregation Rate and Fractal Dimension of Fullerene Nanoparticles via Simultaneous Multiangle Static and Dynamic Light Scattering Measurement. *J. Colloid Interface Sci.* **2013**, *392*, 27–33. https://doi.org/10.1016/j.jcis.2012.09.088.
(34) Wahl, A.; Le Juge, C.; Davranche, M.; El Hadri, H.; Grassl, B.; Reynaud, S.; Gigault, J. Nanoplastic Occurrence in a Soil Amended with Plastic Debris. *Chemosphere* **2021**, *262*, 127784. https://doi.org/10.1016/j.chemosphere.2020.127784.
(35) Abécassis, B.; Cottin-Bizonne, C.; Ybert, C.; Ajdari, A.; Bocquet, L. Boosting Migration of Large Particles by Solute Contrasts. *Nat. Mater.* **2008**, *7* (10), 785–789. https://doi.org/10.1038/nmat2254.
(36) Ebel, J. P.; Anderson, J. L.; Prieve, D. C. Diffusiophoresis of Latex Particles in Electrolyte Gradients. *Langmuir* **1988**, *4* (2), 396–406. https://doi.org/10.1021/la00080a024.
(37) Salmon, J.-B.; Ajdari, A. Transverse Transport of Solutes between Co-Flowing Pressure-Driven Streams for Microfluidic Studies of Diffusion/Reaction Processes. *J. Appl. Phys.* **2007**, *101* (7), 074902. https://doi.org/10.1063/1.2714773.
(38) Dersoir, B.; de Saint Vincent, M. R.; Abkarian, M.; Tabuteau, H. Clogging of a Single Pore by Colloidal Particles. *Microfluid. Nanofluidics* **2015**, *19* (4), 953–961. https://doi.org/10.1007/s10404-015-1624-y.